Lattice micropatterning of electron microscopy grids for improved cellular cryo-electron tomography throughput

Leeya Engel[a,1], Claudia G. Vasquez[a,1], Elizabeth A. Montabana[b], Belle M. Sow[a], Marcin P. Walkiewicz[c], William I. Weis[d], and Alexander R. Dunn[a] ✉

[a]Department of Chemical Engineering, Stanford University, Stanford, CA 94305
[b]Stanford-SLAC CryoEM Initiative, Stanford, CA 94305
[c]Cell Sciences Imaging Facility, Stanford University, Stanford, CA 94305
[d]Departments of Structural Biology and Molecular and Cellular Physiology, Stanford University School of Medicine, Stanford, CA 94305
[1]Equal contributing authors

Cryo-electron tomography is the highest resolution tool available for structural analysis of macromolecular complexes within their native cellular environment. At present, data acquisition suffers from low throughput, in part due to the low probability of positioning a cell such that the subcellular structure of interest is on a region of the electron microscopy (EM) grid that is suitable for imaging. Here, we leverage photo-micropatterning of EM grids to optimally position endothelial cells to enable high-throughput imaging of cell-cell contacts. This method increases the distance between contacts and the thicker cell nuclei such that the regions of interest are sufficiently thin for imaging. The resulting pipeline enables the observation of a diverse array of structures at endothelial cell-cell contacts, demonstrating the utility of this technique in enhancing the rate of data acquisition for cellular cryo-electron tomography studies.

cryoET | cryo-EM | micropatterning | bioengineering
Correspondence: ***alex.dunn@stanford.edu***

Introduction

Cryo-electron tomography (cryoET) is a three dimensional electron microscopy (EM) technique uniquely capable of imaging the interior of frozen cells at the nanometer scale (1–4). While other EM techniques have contributed to our understanding of macromolecular organization in cells, they do not maintain macromolecules in their native state within a hydrated cell. For example, platinum replica electron microscopy is a productive technique for studying cytoskeletal organization, but it strips away the cell membrane and introduces artifacts associated with dehydration and chemical fixation (5). Preservation of the membrane, cytoskeletal structure and associated proteins makes cryoET particularly suited to assessing the ultrastructure of cell-cell contacts.

CryoET is limited by the throughput of data collection as it is time consuming to collect a sufficient number of high-quality tilt-series (6). This low throughput has a number of sources, including the mechanical limitations of the stage requiring refocusing, the software operating the microscope, and the ability to locate the region of interest. The latter issue is particularly limiting for *in situ* cryoET due to the improbability of a cell or a subcellular region of interest being fortuitously positioned in an imageable region of the EM grid. We and others have addressed this limitation by applying photo-micropatterning to confine single cells to extracellular matrix (ECM) islands centrally positioned on grid-squares (7, 8). Micropatterning EM grids to shape and position single cells facilitated cell thinning by cryo-focused ion beam milling (cryo-FIB) and *in situ* cryoET (8). Cryo-FIB requires expensive, specialized machinery that is not widely available, and moreover severely restricts experimental throughput due to its slow speed and complexity.

Here we use EM grid micropatterning to create a continuous ECM lattice that promotes the assembly of thin cell-cell contacts in imageable regions of EM grids. Importantly, the lattice micropattern directs the thicker cell nuclei away from the centers of EM grid-squares such that cell-cell contacts are sufficiently thin for imaging by cryoET.

As a proof of concept, we applied this technique to optimize cryoET sample preparation of contacts between endothelial cells. A longstanding challenge has been to visualize the formation and remodeling of cell-cell junctions in endothelial cells (ECs). ECs line the vasculature and actively remodel their intercellular junctions during inflammation, wound healing and vessel remodeling. Despite their critical importance to vascular health, relatively little is known about the earliest and latest stages of cell-cell junction formation and dissassembly, as the ultrastructure of remodeling junctions is difficult to study using conventional imaging modalities. We found that taking *in situ* cryoET sample preparation from a trial-and-error art to a controlled and reproducible process facilitated high resolution imaging of intact EC cell-cell contacts and revealed a rich variety of sub-cellular structures within contacting cellular protrusions. More generally, this study sets the stage for structural studies of a variety of other systems such as neuronal and immunological synapse formation, where cellular structures can be localized to the cell periphery, by refining techniques that dramatically increase the efficiency of *in situ* cryoET data acquisition.

Results and Discussion

To improve the workflow of *in situ* cryoET, we micropatterned EM grids with a continuous lattice of ECM aligned to the grid bars. The higher availability of ECM at inter-

DRAFT

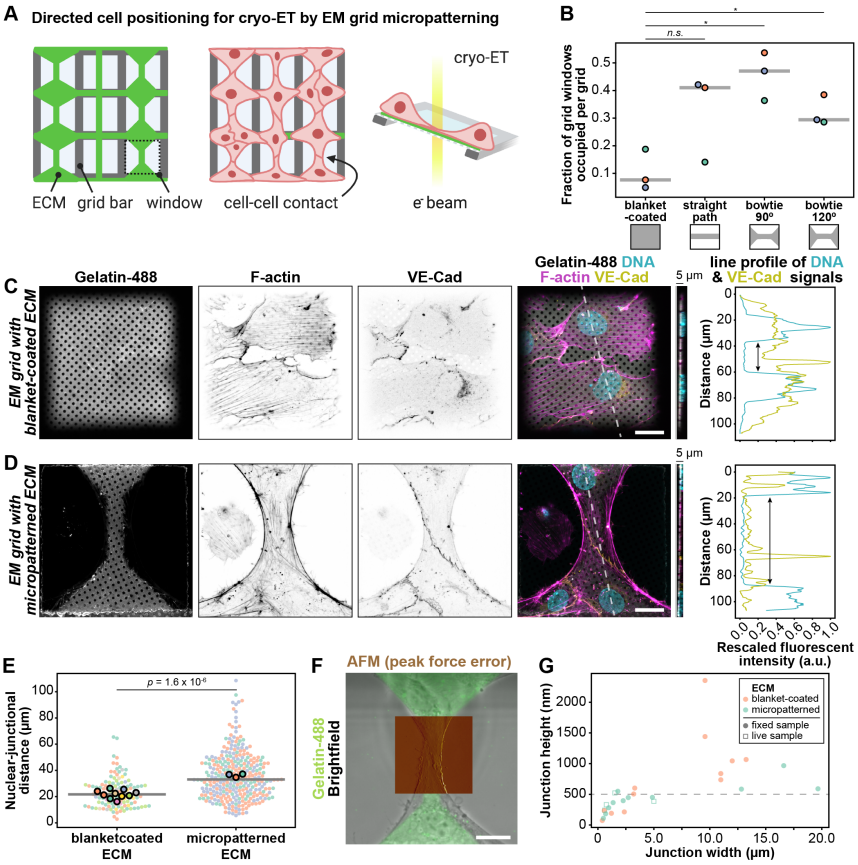

Fig. 1. Lattice micropatterning improves throughput for cryo-ET of cell-cell contacts. (A) Schematic shows ECM lattice micropattern positioning cell-cell contacts on an EM grid. ECM lattice (green) directs the assembly of cell-cell contacts toward grid-square centers. (B) Micropatterning increased the number of optimally positioned cell-cell junctions per EM grid. Median for all measurements indicated by the gray line. N = 3 grids for each ECM condition. Welch's *t* tests: *P < 0.05; ns = not significant. (C, D) Representative image of fixed ECs on EM grids blanket-coated (C) and micropatterned (D) with Oregon Green 488-gelatin, and immunostained for F-actin, VE-Cad and DNA. Dashed line indicates position of the Z-stack reslice and line profile of DNA (teal) and VE-cad signals (green). (E) Lattice micropatterning increased the distance between nuclei and cell-cell junctions. Each point represents an individual measurement of nuclear-junctional distance and each color represents a different EM grid. The mean of the measurements from each grid is indicated by a point outlined in black. Median for all measurements is indicated by the gray line. N = 10 grids, 120 measurements for blanket-coated condition, N = 3 grids, 320 measurements for micropatterned condition. P-value calculated using Welch's *t* test comparing grid replicates. (F) Representative brightfield image of ECs on micropatterned glass (grayscale) overlaid with fluorescence image to show micropattern (green). Inset (AFM peak force error) shows the topography of the cell-cell contact. (G) EC cell-cell contacts can be below 500 nm, the thickness threshold for cryo-EM (3). Measurements from AFM scans show the heights and widths of EC cell-cell contacts on blanket-coated (orange) and micropatterned (green) glass samples. Scale bars, 20 µm.

section points between ECM tracks on the micropatterns attracted the thick cell bodies, promoting the availability of thin cell protrusions for imaging (Fig. 1A). The lattice contained three micropattern variations. "Straight" micropatterns consisted of 10 µm wide intersecting tracks, while "bowtie" micropatterns consisted of 10 µm tracks that widened into 90° or 120° angle diamond shapes at ECM track intersections. We compared the number of cell-cell contacts on imageable regions of EM grids that were blanket-coated with ECM to the number of cell-cell contacts on imageable regions of EM grids that were micropatterned with an ECM lattice (Fig. 1B). Cell-cell contacts were present on only 10.4 +/- 4.2 (S.E.M.)% of grid-squares on EM grids that were blanket-coated with ECM (Fig. 1B-C). In contrast, cell-cell contacts were present on an average of 32.4 +/- 9.1 (S.E.M.)% of grid-squares for straight ECM micropatterns, 45.7 +/- 5.0 (S.E.M.)% of grid-squares for 90° bowtie micropatterns, and 32.1 +/- 3.1 (S.E.M.) for micropatterns with 120° bowtie micropatterns. In addition to significantly increasing the number of grid-squares occupied by cell-cell contacts, lattice micropatterning increased the distance between thick nuclei and intercellular junctions (Fig. 1C-E), improving the likelihood of a well-positioned cell-cell contact falling below the 500 nm thickness threshold for direct imaging (3). We noted an anecdotal relationship between cell-cell contact width and height. Cell-cell contacts below 500 nm thick were also below 10 µm wide for both micropatterned and blanket-coated EM grids (Fig. 1G).

Lattice micropatterned EM grids generated reproducible cellular samples for cryoET. The grid atlas in Fig. 2A shows how lattice micropatterning can be used to orient cells (vertically or horizontally) on grid-squares, potentially enabling the programming of visual labels for correlative EM techniques. For example, orienting cells in a single quadrant of the grid perpendicular to the direction of the cells in the other quadrants makes the location of the grid center apparent during TEM, enabling correlation with grid maps generated by light microscopy. In our hands, lattice micropatterning led to a dramatic increase in the ease of data acquisition. Once we had established optimal cell seeding density and freezing parameters, we found that we did not need to screen vitrified grids prior to imaging as is typically required in order to identify a sufficient number of cellular subregions suitable for imaging.

We were surprised by the structural variety of filamentous (F) actin-rich membrane protrusions at endothelial cell-cell contacts (Fig. 2C-G). While a number of reconstructed tomograms depict what appear to be endothelial adherens junctions based on the literature (9) (Fig. 2C and E), many tomograms revealed thin, intersecting membrane protrusions between cells. These structures appear less rigid than expected for filopodia initiating cell-cell contact (Fig. 2D). Their function is not immediately clear: They may be thin fibers initiating contact, retraction fibers between parting cells, migrasomes left by retreating cells, or suspended protrusions transferring cargo between cells. In addition, we observed a range of vesicle shapes and sizes at endothelial cell-cell contacts (Fig. 2E-G), both within and outside of the

DRAFT

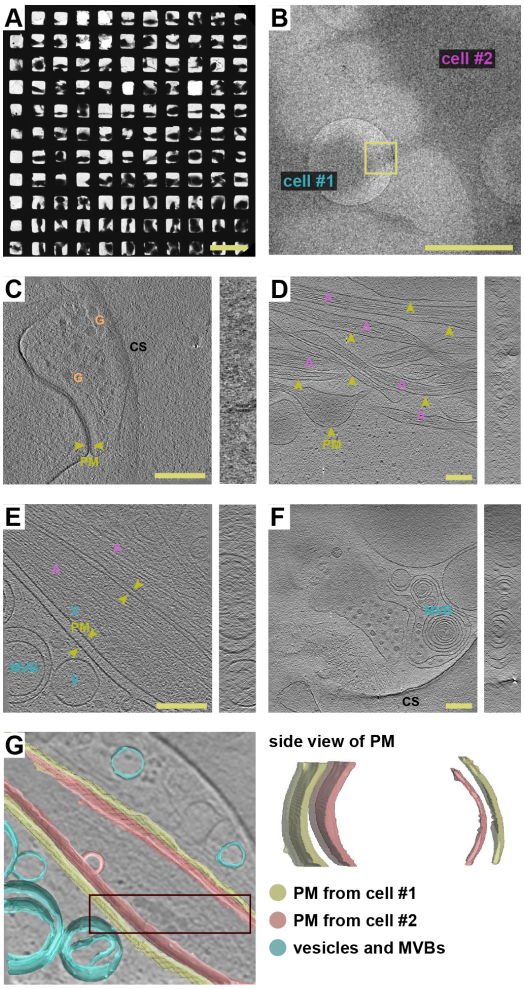

Fig. 2. Lattice micropatterning facilitates *in situ* cryoET of cell-cell contacts. (A) Representative cryo-TEM grid atlas of ECs adhering to a lattice micropatterned EM grid. Cells on the bottom two rows are oriented vertically, as dictated by the micropattern, providing automatic orientation as to the grid location. Scale bar, 200 µm. (B) Magnified cryo-TEM micrograph shows a representative region of interest for the acquisition of a tilt series (yellow box). Scale bar, 2 µm. (C-F) Tomographic slices depict a diversity of membranous structures at cell-cell contacts. *A* actin (purple), *PM* plasma membrane (cyan), *V* vesicle (green), *MVB* multivesicular body (green), *G* granule (orange), *CS* carbon support. (C,E) Membrane-membrane interactions between cellular protrusions. (C) Tomographic slice of the region specified in (B). (D) Thin, intersecting membrane protrusions. (F) Multivesicular bodies. Scale bars, 200 nm. For full tomograms, see SI. (G) Annotated membranes from (E).

plasma membrane. It seems likely that at least some of the structures we captured represent intercellular adherens junctions (9). However, additional investigation will be required to uncover the identity and function of the structures we observed.

Materials and Methods

Cell culture. We cultured human umbilical vein endothelial cells (ECs, cat. C2591A, Lonza Corporation, Walkdersville, MD) in EGM-2 MV Microvascular Endothelial Cell Growth Medium containing EBM-2 basal medium (Lonza cat. CC3156) and supplemented with penicillin (50 units/mL) and streptomycin (50 µg/ml, Life Technologies, Carlsbad, CA) and the following chemicals from the EGM-2MV BulletKit (Lonza cat. CC-4147): hEGFP, VEGF, hFGF-B, R3-IGF-1, hydrocortisone, and ascorbic acid and 5% FBS. We cultured cells on dishes that were precoated with 0.2% gelatin for > 1 h (Sigma-Aldrich, Saint Louis, MO), and maintained them at at 37°C and 5% CO_2. We used cells between passages 7 and 12.

Micropatterning. For biopassivation of EM grids, we placed the grids carbon-side-up on silicone pads (Specialty Manufacturing, Inc., Saginaw, MI) on glass coverslips and exposed them to atmospheric plasma for 10 sec at 30 W (PE-50, Plasma Etch, Carson City, NV). We then incubated the grids in a 100 µg/ml solution of poly(l-lysine)-graft-poly(ethylene glycol)(PLL(20)-g[3.5]-PEG(2)) (SuSoS AG, Dübendorf, Switzerland) in phosphate buffered saline (PBS) for 1 h and rinsed them in PBS.

For photo-micropatterning, we inserted custom silicone stickers into glass bottom dishes to create circular wells 4 mm in diameter (Silhouette CAMEO 3, Silhouette America, Inc., UT). We deposited 25 µL of UV-sensitive photoinitiator (PLPP, Alvéole, Paris, France) into each well and inserted an EM grid carbon-face-down at a 45° angle into the PLPP droplet. We then placed the glass-bottom dish on the stage of a Leica DMi8 outfitted with an Alvéole PRIMO maskless UV-patterning system. We exposed each grid at 2500 mJ/mm^2 with the lattice micropattern (SI). We used the Leonardo software to tile the micropattern to pattern 12x12 grid-square regions (22min/grid). We then rinsed each grid in PBS and then inserted them carbon-side up into 25 µL droplets of 0.2% gelatin in BSA bead solution spiked with 10% by volume 1 mg/mL gelatin-Oregon Green 488 conjugate (G13186, Thermo-Fisher Scientific), contained in a 4 mm silicone well. After 1 h at $\approx$ 22°C, we rinsed the grids in PBS and maintained them at at 37°C until cell seeding.

Cell seeding on micropatterned grids. To obtain the desired distribution of ECs, we suspended cells from an 80% confluent T25 into a 1:8 dilution in media. We replaced the PBS on each grid with 10 µL of media and then added 5 µL of cell suspension at a time until observing $\approx$ 2 cells/grid-square. After 2 h of incubation, we added 2 mL of warm media to each 35 mm dish and vitrified or fixed the samples after an additional 10-14 h.

Immunofluorescence and light microscopy. We fixed ECs with 4% paraformaldehyde in PBS for 15 min at $\approx$ 22 ^{o}C. We blocked and permeabilized the ECs in antibody dilution buffer (ADB) made of 0.1% Triton, 1% bovine serum albumin (BSA, Sigma) in PBS for 1 h at $\approx$ 22 ^{o}C. We incubated the ECs in a 1:500 primary antibody solution containing Mouse anti-CD144 (VE-Cad, BD Pharmingen Cat. #55561) in ADB overnight at 4 ^{o}C, and in secondary antibody solution containing Goat anti-mouse IgG Alexa Fluor 647 (Cell Signaling Technology, Cat. #4410) at a 1:1000 dilution in ADB for 1-2 h at $\approx$ 22 ^{o}C. To the latter solution we added Hoechst solution (34580, Thermo-Fisher Scientific) at a 1:1000 dilution to identify nuclei and ActinRed 555 Read Probest reagent (R37112, Thermo-Fisher Scientific) at

DRAFT

1 drop/mL to stain F-actin. Images in Fig. 1C-D were acquired at 22 ^{o}C using an inverted Zeiss LSM 780 confocal microscope with a 40X/1.3 NA C-Apo water objective, 405 nm diode laser, 561 nm diode laser, 633 nm HeNe laser, and a pinhole setting between 1 and 2 Airy Units. All images were acquired using Zen Black software (Carl Zeiss). Images used for Fig. 1B,E were acquired on an inverted Nikon Ti-E microscope equipped with a Heliophor light engine (89 North) and an Andor sCMOS Neo camera using a 20x Plan Apo Lambda air objective lens.

Atomic force microscopy. We performed atomic force microscopy on live and fixed cells cultured on glass bottom dishes pretreated with gelatin using a BioScope Resolve BioAFM in PeakForce QNM mode and a PFQNM-LC-A-CAL cantilever (Bruker, Santa Barbara, CA). We measured cell-cell contact heights from the height sensor channel using Nanoscope Analysis 1.9. The AFM was mounted on top of a Zeiss Axio Observer Z1 inverted epifluorescent microscope outfitted with a 20x objective.

Vitrification, cryoET, and tomogram reconstruction. We vitrified cells using a Leica EM GP plunge freezer. Immediately prior to plunge-freezing, we added 3 uL of AuNP solution to each grid (Aurion BSA Gold tracer 10 nm, Fisher Cat. 50-248-12). The gold side of the grid was blotted for 1.3-1.5 sec before the grid was plunged into liquid nitrogen - cooled ethane. We clipped the grids into autogrids for automatic handling by the FEI Krios G2 transmission electron microscope (TEM). The TEM was equipped with an energy filter and a K2 direct electron detector (Gatan). We used SerialEM software (10) to operate the TEM at 300 kV in low-dose mode and acquire tilt series at a magnification of 33,000x (0.4315 nm/px). We also collected tilt series at a magnification of 64,000x (0.2235 nm/px), using a Volta phase plate to improve image contrast (11). We motion corrected images with MotionCor2 software (12), aligned them using gold fiducials, and reconstructed tomograms using the IMOD software package, version 4.9.1 (13). 3D segmentation of the tomogram volume in Fig. 2G was performed using Amira (FEI/Thermo Fisher Scientific) software.

Acknowledgements

We thank Dunn lab members for helpful discussion, M. Azubel for advice on cell preparation for cryoET, and R.G. Held and J. Leitz for advice on drift correction and tomogram reconstruction. The project described was supported, in part, by Award Number 1S10OD021514-01 from the National Center for Research Resources (NCRR). Its contents are solely the responsibility of the authors and do not necessarily represent the official views of the NCRR or the NIH. Work was performed in part in the nano@Stanford labs, which are supported by the National Science Foundation as part of the National Nanptechnology Coordinated Infrastructure under award ECCS-1542152. Fig 1A was created with BioRender.com. This work was supported by NIH F32GM125113 (CGV), R01HL128779 (ARD), R35GM130332 (ARD), R35GM131747 (WIW), and an HHMI Faculty Scholars Award (ARD).

References

1. Ohad Medalia, Igor Weber, Achilleas S Frangakis, Daniela Nicastro, Günther Gerisch, and Wolfgang Baumeister. Macromolecular architecture in eukaryotic cells visualized by cryo-electron tomography. *Science*, 298(5596):1209–1213, 2002.
2. Shoh Asano, Benjamin D Engel, and Wolfgang Baumeister. In situ cryo-electron tomography: a post-reductionist approach to structural biology. *Journal of molecular biology*, 428 (2):332–343, 2016.
3. Lu Gan and Grant J Jensen. Electron tomography of cells. *Quarterly reviews of biophysics*, 45(1):27–56, 2012.
4. Saikat Chakraborty, Marion Jasnin, and Wolfgang Baumeister. Three-dimensional organization of the cytoskeleton: a cryo-electron tomography perspective. *Protein Science*, 2020.
5. Tatyana M Svitkina. Platinum replica electron microscopy: Imaging the cytoskeleton globally and locally. *The international journal of biochemistry & cell biology*, 86:37–41, 2017.
6. W Wan and JAG Briggs. Cryo-electron tomography and subtomogram averaging. In *Methods in enzymology*, volume 579, pages 329–367. Elsevier, 2016.
7. Leeya Engel, Guido Gaietta, Liam P Dow, Mark F Swift, Gaspard Pardon, Niels Volkmann, William I Weis, Dorit Hanein, and Beth L Pruitt. Extracellular matrix micropatterning technology for whole cell cryogenic electron microscopy studies. *Journal of Micromechanics and Microengineering*, 29(11):115018, sep 2019. doi: 10.1088/1361-6439/ab419a.
8. Mauricio Toro-Nahuelpan, Ievgeniia Zagoriy, Fabrice Senger, Laurent Blanchoin, Manuel Théry, and Julia Mahamid. Tailoring cryo-electron microscopy grids by photo-micropatterning for in-cell structural studies. *Nature Methods*, 17(1):50–54, 2020.
9. Nadia Efimova and Tatyana M Svitkina. Branched actin networks push against each other at adherens junctions to maintain cell–cell adhesion. *Journal of Cell Biology*, 217(5):1827–1845, 2018.
10. David N Mastronarde. Automated electron microscope tomography using robust prediction of specimen movements. *Journal of structural biology*, 152(1):36–51, 2005.
11. Radostin Danev, Bart Buijsse, Maryam Khoshouei, Jürgen M Plitzko, and Wolfgang Baumeister. Volta potential phase plate for in-focus phase contrast transmission electron microscopy. *Proceedings of the National Academy of Sciences*, 111(44):15635–15640, 2014.
12. Shawn Q Zheng, Eugene Palovcak, Jean-Paul Armache, Kliment A Verba, Yifan Cheng, and David A Agard. Motioncor2: anisotropic correction of beam-induced motion for improved cryo-electron microscopy. *Nature methods*, 14(4):331–332, 2017.
13. James R Kremer, David N Mastronarde, and J Richard McIntosh. Computer visualization of three-dimensional image data using imod. *Journal of structural biology*, 116(1):71–76, 1996.

DRAFT